

to appear in *The Astrophysical Journal*

On Radiation Pressure in Static, Dusty H II Regions

B.T. Draine

Princeton University Observatory, Peyton Hall, Princeton, NJ 08544;

`draine@astro.princeton.edu`

ABSTRACT

Radiation pressure acting on gas and dust causes H II regions to have central densities that are lower than the density near the ionized boundary. H II regions in static equilibrium comprise a family of similarity solutions with 3 parameters: β , γ , and the product $Q_0 n_{\text{rms}}$; β characterizes the stellar spectrum, γ characterizes the dust/gas ratio, Q_0 is the stellar ionizing output (photons/s), and n_{rms} is the rms density within the ionized region. Adopting standard values for β and γ , varying $Q_0 n_{\text{rms}}$ generates a one-parameter family of density profiles, ranging from nearly uniform-density (small $Q_0 n_{\text{rms}}$) to shell-like (large $Q_0 n_{\text{rms}}$). When $Q_0 n_{\text{rms}} \gtrsim 10^{52} \text{ cm}^{-3} \text{ s}^{-1}$, dusty H II regions have conspicuous central cavities, even if no stellar wind is present. For given β , γ and $Q_0 n_{\text{rms}}$, a fourth quantity, which can be Q_0 , determines the overall size and density of the H II region. Examples of density and emissivity profiles are given. We show how quantities of interest – such as the peak-to-central emission measure ratio, the rms-to-mean density ratio, the edge-to-rms density ratio, and the fraction of the ionizing photons absorbed by the gas – depend on β , γ , and $Q_0 n_{\text{rms}}$. For dusty H II regions, compression of the gas and dust into an ionized shell results in a substantial increase in the fraction of the stellar photons that actually ionize H (relative to a uniform density H II region with the same dust/gas ratio and density $n = n_{\text{rms}}$). We discuss the extent to which radial drift of dust grains in H II regions can alter the dust-to-gas ratio. The applicability of these solutions to real H II regions is discussed.

Subject headings: ISM: bubbles; dust, extinction; HII regions; ISM: structure; infrared: ISM; radio continuum: ISM

1. Introduction

Strömgren (1939) idealized photoionized nebulae around hot stars as static, spherical regions with a uniform density of ionized gas out to a bounding radius R . The Strömgren sphere model continues to serve as the starting point for studies of H II regions around hot stars. However, a number of physical effects lead to departures from the simple Strömgren sphere model: dynamical expansion of the H II region if the pressure in the surrounding neutral medium cannot confine the

ionized gas; deviations from sphericity due to nonuniform density; motion of the star relative to the gas; injection of energy and momentum by a stellar wind; absorption of H-ionizing photons by dust grains; and radiation pressure acting on gas and dust. Each of these effects has been the object of a number of investigations, beginning with the study of ionization fronts by Kahn (1954).

Savedoff & Greene (1955) appear to have been the first to discuss the expansion of a spherical H II region in an initially uniform neutral medium. Mathews (1967, 1969) and Gail & Sedlmayr (1979) calculated the dynamical expansion of an H II region produced by an O star in a medium that was initially neutral, including the effects of radiation pressure acting on the dust. Mathews (1967, 1969) showed that radiation pressure on dust would produce low-density central cavities in H II regions. More recently, Krumholz & Matzner (2009) reexamined the role of radiation pressure on the expansion dynamics of H II regions, concluding that radiation pressure is generally unimportant for H II regions ionized by a small number of stars, but is important for the expansion dynamics of giant H II regions surrounding clusters containing many O-type stars. Their study concentrated on the forces acting on the dense shell of neutral gas and dust bounding the H II region, hence they did not consider the density structure within the ionized region.

Dust absorbs $h\nu > 13.6\text{ eV}$ photons that would otherwise be able to ionize hydrogen, thereby reducing the extent of the ionized zone. Petrosian et al. (1972) developed analytic approximations for dusty H II regions. They assumed the gas density to be uniform, with a constant dust-to-gas ratio, and found that dust could absorb a substantial fraction of the ionizing photons in dense H II regions. Petrosian et al. did not consider the effects of radiation pressure.

Dopita et al. (2003, 2006) constructed models of compact H II regions, including the effects of radiation pressure on dust, and presented models for different ionizing stars and bounding pressures. In these models, radiation pressure produces a density gradient within the ionized gas.

The present paper provides a systematic discussion of the structure of dusty H II regions that are assumed to be in equilibrium with an external bounding pressure. The assumptions and governing equations are presented in §2, where it is shown that dusty H II regions are essentially described by a 3-parameter family of similarity solutions. In §3 we show density profiles for selected cases, as well as surface brightness profiles. The characteristic ionization parameter $U_{1/2}$ and the fraction $(1 - f_{\text{ion}})$ of the ionizing photons absorbed by dust are calculated. Dust grain drift is examined in §4, where it is shown that it can alter the dust-to-gas ratio in the centers of high density H II regions. The results are discussed in §5, and summarized in §6.

2. Equilibrium Model

Consider the idealized problem of a static, spherically-symmetric equilibrium H II region ionized by a point source, representing either a single star or a compact stellar cluster. Assume a constant dust-to-gas ratio (the validity of this assumption will be examined later). For simplicity, ignore scattering, and assume σ_d , the dust absorption cross section per H nucleon, to be independent

of photon energy $h\nu$ over the ~ 5 eV to ~ 30 eV range containing most of the stellar power.

Let the star have luminosity $L = L_n + L_i = L_{39}10^{39}$ ergs s^{-1} , where L_n and L_i are the luminosities in $h\nu < 13.6$ eV and $h\nu > 13.6$ eV photons, respectively. The rate of emission of $h\nu > 13.6$ eV photons is $Q_0 \equiv 10^{49}Q_{0,49}$ s^{-1} and the mean energy of the ionizing photons is $\langle h\nu \rangle_i \equiv L_i/Q_0$. A single main sequence star of spectral type O6V has $L_{39} = 0.80$ and $Q_{0,49} = 0.98$ (Martins et al. 2005). A compact cluster of OB stars might be treated as a point source with much larger values of $Q_{0,49}$ and L_{39} .

Ignore He, and assume the H to be nearly fully ionized, with photoionization balancing ‘‘Case B’’ radiative recombination, with ‘‘on-the-spot’’ absorption of $h\nu > 13.6$ eV recombination radiation. Take the effective radiative recombination coefficient to be $\alpha_B \approx 2.56 \times 10^{-13}T_4^{-0.83}$ $\text{cm}^3 \text{s}^{-1}$ for $0.5 \lesssim T_4 \lesssim 2$, with $T_4 \equiv T/10^4$ K, where T is the gas temperature.

Assume the gas to be in dynamical equilibrium (the neutral gas outside the ionized zone is assumed to provide a confining pressure). Static equilibrium then requires that the force per unit volume from radiation pressure be balanced by the pressure gradient:

$$n\sigma_d \frac{[L_n e^{-\tau} + L_i \phi(r)]}{4\pi r^2 c} + \alpha_B n^2 \frac{\langle h\nu \rangle_i}{c} - \frac{d}{dr} (2nkT) = 0 \quad , \quad (1)$$

where $n(r)$ is the proton density, $L_i \phi(r)$ is the power in $h\nu > 13.6$ eV photons crossing a sphere of radius r , and $\tau(r)$ is the dust absorption optical depth. Eq. (1) underestimates the radiation pressure force, because it assumes that recombination radiation (including Lyman- α) and cooling radiation escape freely.

The functions $\phi(r)$ and $\tau(r)$ are determined by

$$\frac{d\phi}{dr} = -\frac{1}{Q_0} \alpha_B n^2 4\pi r^2 - n\sigma_d \phi \quad , \quad (2)$$

$$\frac{d\tau}{dr} = n\sigma_d \quad , \quad (3)$$

with boundary conditions $\phi(0) = 1$ and $\tau(0) = 0$. Define a characteristic density and length scale

$$n_0 \equiv \frac{4\pi\alpha_B}{Q_0} \left(\frac{2ckT}{\alpha_B \langle h\nu \rangle_i} \right)^3 = 4.54 \times 10^5 \frac{T_4^{4.66}}{Q_{0,49}} \left(\frac{18 \text{ eV}}{\langle h\nu \rangle_i} \right)^3 \text{ cm}^{-3} \quad , \quad (4)$$

$$\lambda_0 \equiv \frac{Q_0}{4\pi\alpha_B} \left(\frac{\alpha_B \langle h\nu \rangle_i}{2ckT} \right)^2 = 2.47 \times 10^{16} \frac{Q_{0,49}}{T_4^{2.83}} \left(\frac{\langle h\nu \rangle_i}{18 \text{ eV}} \right)^2 \text{ cm} \quad , \quad (5)$$

and the dimensionless parameters

$$\beta \equiv \frac{L_n}{L_i} = \frac{L}{L_i} - 1 = 3.47 \frac{L_{39}}{Q_{0,49}} \left(\frac{18 \text{ eV}}{\langle h\nu \rangle_i} \right) - 1 \quad , \quad (6)$$

$$\gamma \equiv \left(\frac{2ckT}{\alpha_B \langle h\nu \rangle_i} \right) \sigma_d = 11.2 T_4^{1.83} \left(\frac{18 \text{ eV}}{\langle h\nu \rangle_i} \right) \left(\frac{\sigma_d}{10^{-21} \text{ cm}^2} \right) \quad . \quad (7)$$

The parameter β , the ratio of the power in non-ionizing photons to the power in photons with $h\nu > 13.6\text{eV}$, depends solely on the stellar spectrum. We take $\beta = 3$ as our standard value, corresponding to the spectrum of a $T_\star = 32000\text{K}$ blackbody, but we also consider $\beta = 2$ ($T_\star = 45000\text{K}$) and $\beta = 5$ ($T_\star = 28000\text{K}$); the latter value might apply to a cluster of O and B stars.

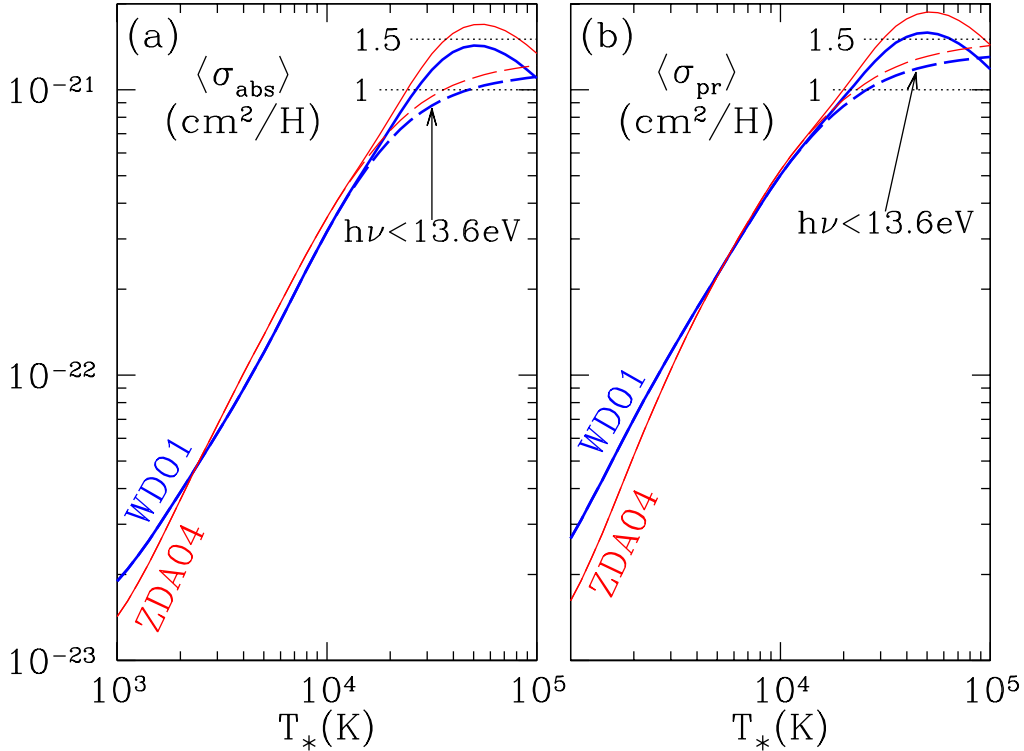


Fig. 1.— (a) Absorption cross section per H, and (b) radiation pressure cross section per H, averaged over blackbody spectra, as functions of the blackbody temperature T_\star , for the dust models of Weingartner & Draine (2001, WD01) and Zubko et al. (2004, ZDA04). Broken lines show averages over $h\nu < 13.6\text{eV}$ only, appropriate for dust in neutral gas.

Momentum can be transferred to a dust grain by photon absorption, but also by scattering. The cross section σ_d appearing in eq. (1) should be $\langle \sigma_{\text{pr}} \rangle$, the radiation pressure cross section per H, $\sigma_{\text{pr}}(\nu) \equiv \sigma_{\text{abs}} + (1 - \langle \cos \theta \rangle) \sigma_{\text{sca}}$, averaged over the spectrum of the radiation field at radius r , where $\sigma_{\text{abs}}(\nu)$ and $\sigma_{\text{sca}}(\nu)$ are the absorption and scattering cross section per H, and $\langle \cos \theta \rangle$ is the mean value of the cosine of the scattering angle θ for photons of frequency ν .

In eqs. (2) and (3), σ_d characterizes the effectiveness of the dust in attenuating the radiation field. While scattering does not destroy the photon, it does increase the probability of the photon undergoing subsequent absorption. Thus, the value of σ_d in eqs. (2) and (3) should exceed $\langle \sigma_{\text{abs}} \rangle$.

Figure 1(a) shows the dust absorption cross section per H nucleon averaged over a blackbody

spectrum, for two dust models (Weingartner & Draine 2001; Zubko et al. 2004) that reproduce the wavelength-dependent extinction in the diffuse interstellar medium using mixtures of PAHs, graphite, and amorphous silicate grains. Fig. 1(b) shows that $\langle\sigma_{\text{pr}}\rangle$, the radiation pressure cross section averaged over blackbody spectra, is only slightly larger than $\langle\sigma_{\text{abs}}\rangle$. Given the uncertainties in the nature of the dust in H II regions, it is reasonable to ignore the distinction between $\langle\sigma_{\text{pr}}\rangle$ and the attenuation cross section and simply take $\sigma_d = \langle\sigma_{\text{pr}}\rangle$ in eq. (1–3).

For dust characteristic of the diffuse ISM, one could take $\langle\sigma_{\text{pr}}\rangle \approx 1.5 \times 10^{-21} \text{ cm}^2 \text{ H}^{-1}$ for $2.5 \times 10^4 \text{ K} \lesssim T_{\text{rad}} \lesssim 5 \times 10^4 \text{ K}$. However, dust within an H II region may differ from average interstellar dust. For example, the small-size end of the size distribution might be suppressed, in which case σ_d would be reduced. Low metallicity galaxies will also have lower values of σ_d , simply because there is less material out of which to form grains. In the present work we will assume a factor ~ 1.5 reduction in σ_d relative to the local diffuse ISM, taking $\sigma_d \approx 1 \times 10^{-21} \text{ cm}^2 \text{ H}^{-1}$ as the nominal value, but larger and smaller values of σ_d will also be considered.

The dimensionless parameter γ (defined in eq. 7) depends also on the gas temperature T and on the mean ionizing photon energy $\langle h\nu \rangle_i$, but these are not likely to vary much for H II regions around OB stars. We take $\gamma = 10$ as a standard value, but will also consider $\gamma = 5$ and $\gamma = 20$. Low-metallicity systems would be characterized by small values of γ .

Switching to dimensionless variables $y \equiv r/\lambda_0$, $u \equiv n_0/n$, the governing equations (1–3) become

$$\frac{du}{dy} = -1 - \gamma (\beta e^{-\tau} + \phi) \frac{u}{y^2} \quad , \quad (8)$$

$$\frac{d\phi}{dy} = -\frac{y^2}{u^2} - \gamma \frac{\phi}{u} \quad , \quad (9)$$

$$\frac{d\tau}{dy} = \frac{\gamma}{u} \quad , \quad (10)$$

with initial conditions $\phi(0) = 1$ and $\tau(0) = 0$. The solutions are defined for $0 < y \leq y_{\text{max}}$, where y_{max} is determined by the boundary condition $\phi(y_{\text{max}}) = 0$. The actual radius of the ionized zone is $R = y_{\text{max}}\lambda_0$. For each solution $u(y)$ the mean density is

$$\langle n \rangle = \frac{3n_0}{y_{\text{max}}^3} \int_0^{y_{\text{max}}} \frac{1}{u} y^2 dy \quad , \quad (11)$$

the root-mean-square density is

$$n_{\text{rms}} \equiv n_0 \left[\frac{3}{y_{\text{max}}^3} \int_0^{y_{\text{max}}} \frac{1}{u^2} y^2 dy \right]^{1/2} \quad , \quad (12)$$

and the gas pressure at the edge of the H II region is

$$p_{\text{edge}} = 2n(R)kT = \frac{2n_0kT}{u(y_{\text{max}})} \quad . \quad (13)$$

Let

$$R_{s0} \equiv \left(\frac{3Q_0}{4\pi n_{\text{rms}}^2 \alpha_B} \right)^{1/3} = 2.10 \times 10^{18} \frac{Q_{0,49}^{1/3}}{n_{\text{rms},3}^{2/3}} T_4^{0.28} \text{ cm} \quad (14)$$

be the radius of a dustless Strömgren sphere with density $n_{\text{rms}} = 10^3 n_{\text{rms},3} \text{ cm}^{-3}$. The fraction of the $h\nu > 13.6 \text{ eV}$ photons that are absorbed by H is simply

$$f_{\text{ion}} = \left(\frac{R}{R_{s0}} \right)^3. \quad (15)$$

For given (β, γ) , varying the initial value¹ of $u = n_0/n$ at some fixed $y = r/\lambda_0$ generates solutions with different density profiles. Therefore the full set of solutions forms a three-parameter family of similarity solutions $u(y)$, $\phi(y)$, and $\tau(y)$, parametrized by β , γ , and a third parameter. The third parameter can be taken to be $Q_0 n_{\text{rms}}$. For dusty H II regions, an alternative choice for the third parameter is the dust optical depth on a path R_{s0} with density n_{rms} :

$$\tau_{d,0} \equiv n_{\text{rms}} R_{s0} \sigma_d = 2.10 (Q_{0,49} n_{\text{rms},3})^{1/3} T_4^{0.28} \frac{\sigma_d}{10^{-21} \text{ cm}^2} \quad (16)$$

$$= 0.188 \gamma (Q_{0,49} n_{\text{rms},3})^{1/3} T_4^{-1.55} \frac{\langle h\nu \rangle_i}{18 \text{ eV}}. \quad (17)$$

The static H II regions described by eq. (1–3) are determined by 7 distinct dimensional quantities: three parameters describing the central star (Q_0 , $\langle h\nu \rangle_i$, and L_n), the recombination rate coefficient α_B , the thermal energy kT , the dust cross section per nucleon σ_d , and the external pressure p_{edge} confining the H II region. According to the present analysis, this 7-parameter family of solutions actually reduces to a 3-parameter family of similarity solutions. The dimensionless parameters β and γ , plus choice of an initial value for the function u near $y = 0$, suffice to determine the scaled density profile $n(r)/n_0$ and radius $y_{\text{max}} = R/\lambda_0$: this is the 3-parameter family of similarity solutions.

Specifying numerical values for the ratios Q_0/α_B and $kT/(\alpha_B \langle h\nu \rangle_i)$ fixes the values of n_0 and λ_0 , thus giving $n(r)$ for $r < R$. Thus far we have invoked 5 independent parameters, but have not actually specified either kT or α_B .

Specifying kT and α_B – the 6th and 7th parameters – allows us to compute the actual values of Q_0 and $\langle h\nu \rangle_i$, and the bounding pressure $p_{\text{edge}} = 2n(R)kT$.

If the “initial value” of u near the origin is taken as a boundary condition, then p_{edge} emerges as a derived quantity. However, if we instead regard p_{edge} as a boundary condition, then the initial value of u ceases to be a free parameter, and instead must be found (e.g., using a shooting technique) so as to give the correct boundary pressure p_{edge} : the initial value of u is thus determined by the 7 physical parameters (Q_0 , $\langle h\nu \rangle_i$, L_n , α_B , T , σ_d , and p_{edge}).

¹ For $\gamma > 0$, $u \propto \exp[(\beta + 1)\gamma/y] \rightarrow \infty$ as $y \rightarrow 0$, and the integration must start at some small $y > 0$.

Thus we see how the 3 parameter family of dimensionless similarity solutions corresponds to a 7 parameter family of physical solutions.

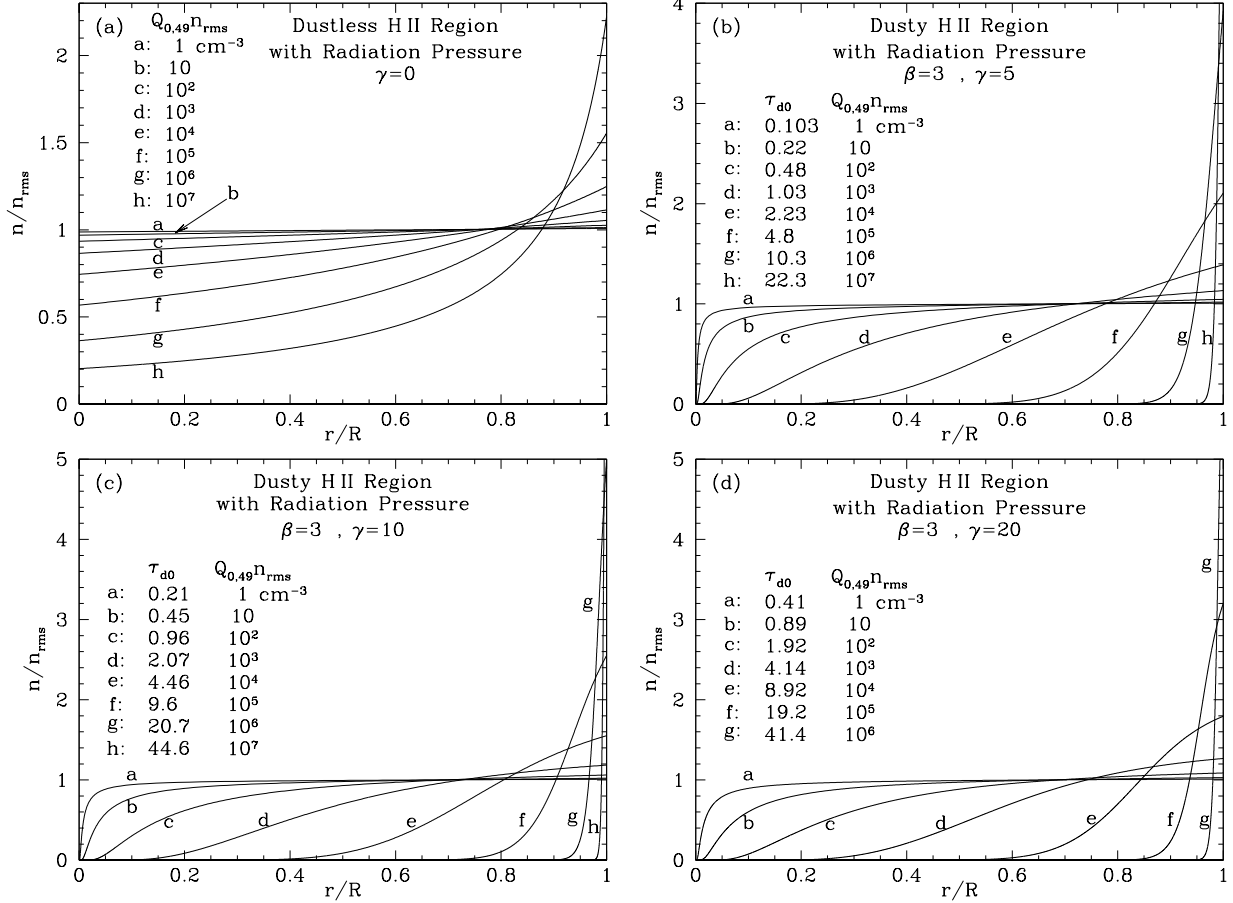


Fig. 2.— Normalized density profiles of static equilibrium H II regions, as a function of r/R , where R is the radius of the ionized region. Profiles are shown for 7 values of $Q_0 n_{\text{rms}}$; the numerical values given in the legends assume $T_4 = 0.94$ and $(h\nu)_i = 18 \text{ eV}$. (a) Dustless ($\gamma = 0$); (b) $\gamma = 5$; (c) $\gamma = 10$; (d) $\gamma = 20$.

3. Results

Equations (8-10) can be integrated numerically. Figure 2a shows the solution for the case where no dust is present ($\gamma = 0$). Radiation pressure associated with photoionization produces a density gradient in the H II region, but it is modest unless $Q_0 n_{\text{rms}}$ is very large. The central density is nonzero. For $Q_{0,49} n_{\text{rms}} \lesssim 10^3 \text{ cm}^{-3}$, the density is uniform to within $\pm 15\%$.

As discussed above, the dust abundance relative to H is characterized by the parameter γ . Density profiles are shown in Fig. 2b-d for $\beta = 3$ and $\gamma = 5, 10, 20$, corresponding approximately to $\sigma_d = 0.5, 1, 2 \times 10^{-21} \text{ cm}^2$. With dust present, the density formally goes to zero at $r = 0$. For fixed

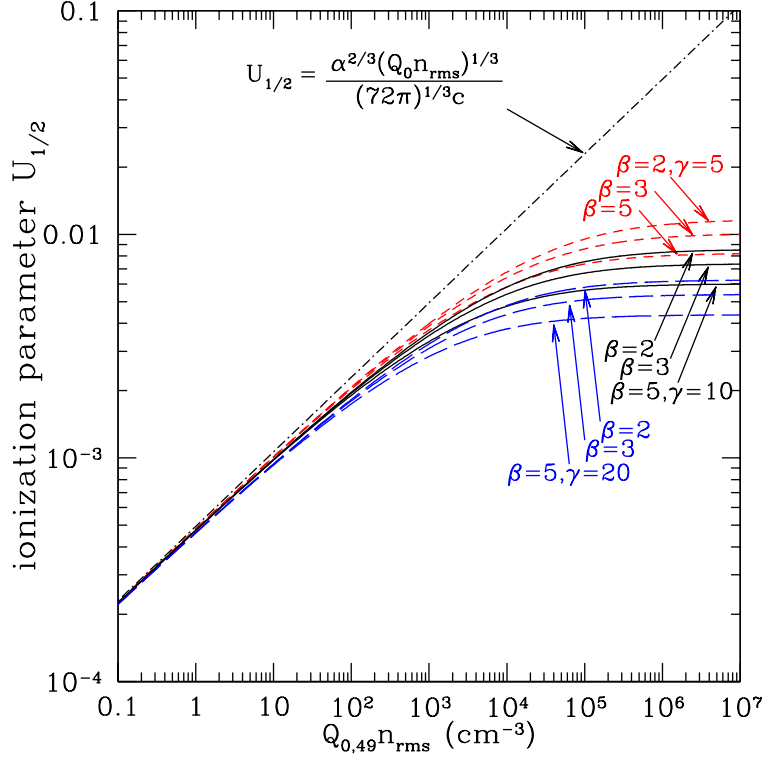


Fig. 3.— Ionization parameter $U_{1/2}$ at the half-ionization radius in dusty H II regions (see text), calculated assuming $T_4 = 0.94$ and $\langle h\nu \rangle_i = 18 \text{ eV}$.

γ , the size of the low-density central cavity (as a fraction of the radius R of the ionization front) increases with increasing $Q_0 n_{\text{rms}}$. The enhancement of the density near the ionization front also becomes more pronounced as $Q_0 n_{\text{rms}}$ is increased. For $\beta = 3$, $\gamma = 10$ and $Q_{0,49} n_{\text{rms}} = 10^5 \text{ cm}^{-3}$, we find $n(R) = 2.5 n_{\text{rms}}$.

The state of ionization of the gas is determined by the hardness of the radiation field, and the value of the dimensionless “ionization parameter”

$$U \equiv \frac{n(h\nu > I_{\text{H}})}{n_{\text{H}}} \quad , \quad (18)$$

where $n(h\nu > I_{\text{H}})$ is the density of photons with $h\nu > I_{\text{H}}$. Within an H II region, the value of U varies radially. As a representative value, we evaluate $U_{1/2}$, the value at the “half-ionization” radius $R_{1/2}$, the radius within which 50% of the H ionizations and recombinations take place.² In

² Some authors (e.g., Dopita et al. 2006) use the volume-averaged ionization parameter $\langle U \rangle_V$. For a uniform density dustless H II region, $\langle U \rangle_V = (81/256\pi)^{1/3} (\alpha_B^{2/3}/c) (Q_0 n_{\text{rms}})^{1/3} = 2.83 U_{1/2}$.

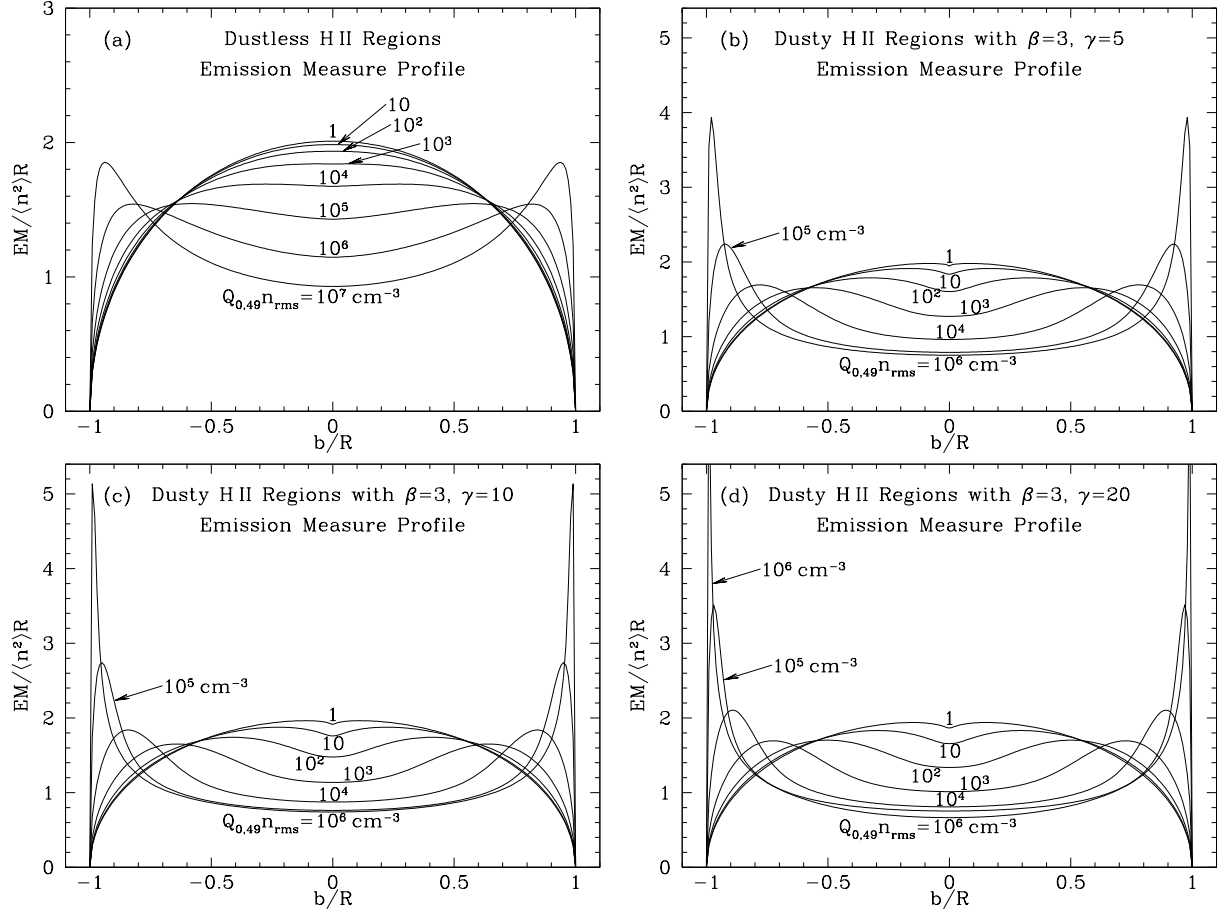


Fig. 4.— Normalized emission measure (EM) profiles for a cut across the center of H II regions with (a) $\gamma = 0$ (no dust), (b) $\gamma = 5$, (c) $\gamma = 10$, and (d) $\gamma = 20$. Profiles are shown for selected values of $Q_0 n_{\text{rms}}$. Numerical values of $Q_{0,49} n_{\text{rms}}$ assume $T_4 = 0.94$ and $\langle h\nu \rangle_i = 18$ eV.

a uniform density dustless H II region, $R_{1/2} = 2^{-1/3} R_{S0}$ is the same as the half-mass radius, and

$$U_{1/2}^{(\text{no dust})} = \frac{\alpha_B^{2/3}}{(72\pi)^{1/3} c} (Q_0 n_{\text{rms}})^{1/3} . \quad (19)$$

For our present models,

$$U_{1/2} = \frac{Q_0}{4\pi\lambda_0^2 n_0 c} \frac{\phi(y_{1/2}) u(y_{1/2})}{y_{1/2}^2} , \quad (20)$$

where $y_{1/2} = R_{1/2}/\lambda_0$ is the value of y within which 50% of the H ionizations and recombinations take place. Figure 3 shows $U_{1/2}$ as a function of $Q_0 n_{\text{rms}}$ for static dusty H II regions with radiation pressure, for selected values of β and γ . For small values of $Q_0 n_{\text{rms}}$, dust and radiation pressure are negligible and $U_{1/2}$ coincides with $U_{1/2}^{(\text{no dust})}$ (eq. 19). However, for large values of $Q_0 n_{\text{rms}}$, $U_{1/2}$ falls below $U_{1/2}^{(\text{no dust})}$. For $\gamma \approx 10$ – corresponding to the dust abundances that we consider to be

likely for Galactic H II regions – we see that $U_{1/2} \approx 0.07 \pm 0.02$ for $Q_{0,49}n_{\text{rms}} \gtrsim 10^4 \text{ cm}^{-3}$.

The emission measure $EM(b) = \int n_e^2 ds$ is shown as a function of impact parameter b in Figure 4. For small values of $Q_0 n_{\text{rms}}$, the intensity profile is close to the semicircular profile of a uniform density sphere. As $Q_0 n_{\text{rms}}$ is increased, the profile becomes flattened, but, if no dust is present ($\gamma = 0$, Fig. 2a), the ionized gas only begins to develop an appreciable central minimum for $Q_{0,49}n_{\text{rms}} \gtrsim 10^{4.5} \text{ cm}^{-3}$.

When dust is present, however, the profiles are strongly affected. For standard parameters $\beta = 3, \gamma = 10$, the emission measure shows a pronounced central minimum for $Q_{0,49}n_{\text{rms}} \gtrsim 10^3 \text{ cm}^{-3}$, with a peak-to-minimum ratio > 2 for $Q_{0,49}n_{\text{rms}} \gtrsim 10^4 \text{ cm}^{-3}$. As $Q_0 n_{\text{rms}}$ is increased, the ionized gas becomes concentrated in a thin, dense shell, the peak intensity near the edge rises, and the central emission measure changes from $EM(0) = 2n_{\text{rms}}^2 R$ for small $Q_0 n_{\text{rms}}$ to $EM(0) \rightarrow (2/3)n_{\text{rms}}^2 R$ as $Q_0 n_{\text{rms}} \rightarrow \infty$.

When $\tau_{d0} \gg 1$, the present models have the ionized gas concentrated in a thin, dense, shell. Figure 5a shows the ratio of the rms density n_{rms} to the mean density $\langle n \rangle$ as a function of τ_{d0} . The highest ionized density occurs at the outer edge of the ionized zone, and Figure 5b shows the ratio $n_{\text{edge}}/n_{\text{rms}}$ as a function of τ_{d0} .

In the low density limit $Q_0 n_{\text{rms}} \rightarrow 0$, the dust optical depth from center to edge $\tau(R) \approx \tau_{d0}$. The actual dust optical depth from center to edge is shown in Figure 5c. When the H II region develops a dense shell, which occurs for $\tau_{d0} \gtrsim 3$, the actual dust optical depth $\tau(R)$ is significantly smaller than the value τ_{d0} . Figure 5c shows that for $\tau_{d0} = 40$, for example, the actual dust optical depth $\tau(R)$ is only in the range 1–2.3, depending on the values of β and γ .

The shell-like structure is also apparent in the ratio of the peak intensity to the central intensity. As seen in Figures 4(b-d), dust causes the peak intensity to be off-center. For fixed β and γ , the ratio of peak intensity to central intensity $I(\text{peak})/I(\text{center})$ increases monotonically with increasing τ_{d0} , as shown in Fig. 5(d).

Because the shell is dense, radiative recombination is rapid, the neutral hydrogen fraction is enhanced, and H atoms can compete with dust to absorb $h\nu > 13.6 \text{ eV}$ photons. Figure 6 shows f_{ion} , the fraction of the $h\nu > 13.6 \text{ eV}$ photons emitted by the star that photoionize H (i.e., are not absorbed by dust), as a function of the parameter τ_{d0} . Results are shown for $\beta = 2, 3, 5$ and $\gamma = 5, 10, 20$. For $2 \leq \beta \leq 5$, $5 \leq \gamma \leq 20$, and $0 \leq \tau_{d0} \leq 40$, the numerical results in Figure 6 can be approximated by the fitting formula

$$f_{\text{ion}}(\beta, \gamma, \tau_{d0}) \approx \frac{1}{1 + (2/3 + AB)\tau_{d0}} + \frac{AB\tau_{d0}}{1 + B\tau_{d0}} \quad (21)$$

$$A = \frac{1}{1 + 0.75\gamma^{0.65}\beta^{-0.44}} \quad (22)$$

$$B = \frac{0.5}{1 + 0.1(\gamma/\beta)^{1.5}} \quad (23)$$

where β , γ , and τ_{d0} are given by (6), (7), and (16). The form of eq. (21-23) has no physical

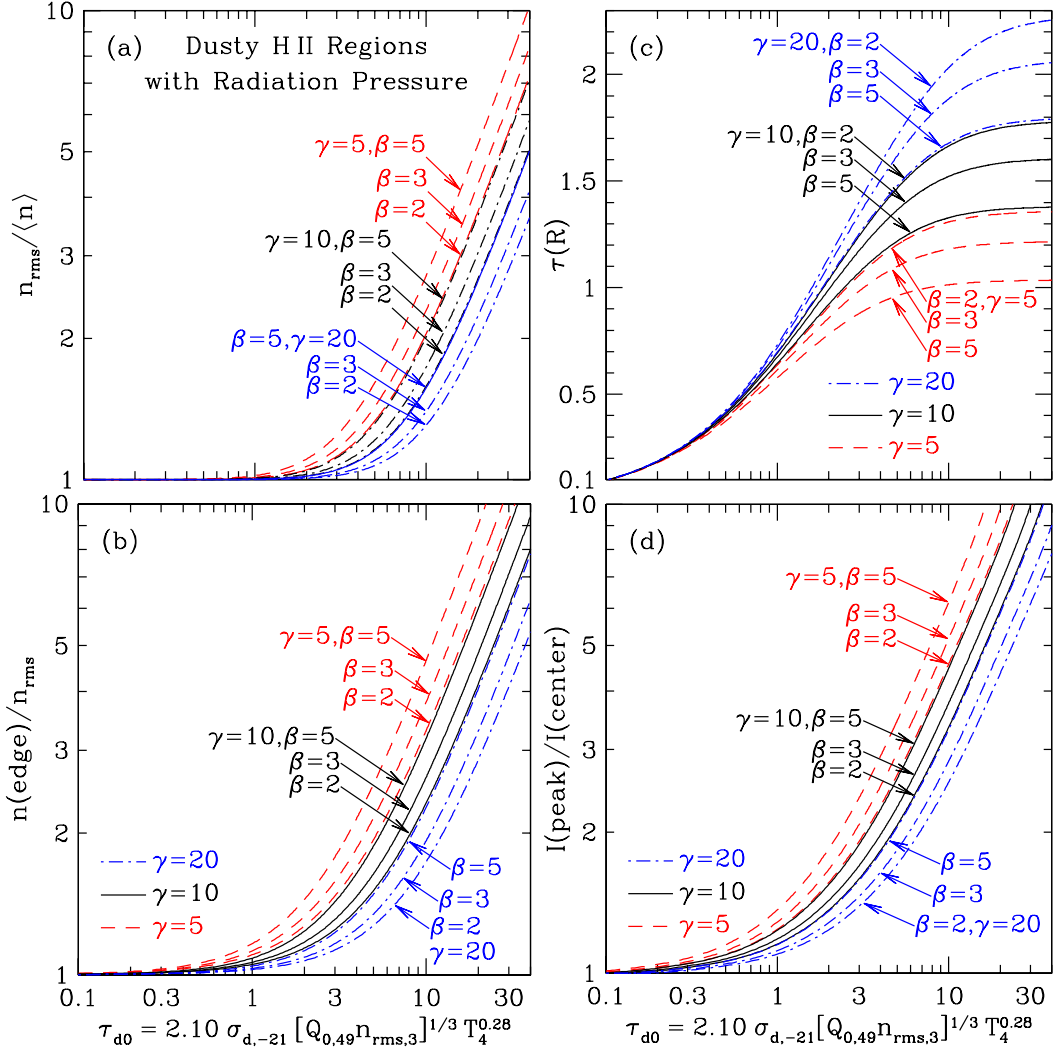


Fig. 5.— For dusty H II regions with $\gamma = 5, 10, 20$ and $\beta = 2, 3, 5$, as a function of τ_{d0} : (a) ratio $n_{\text{rms}}/\langle n \rangle$ of rms density to mean density; (b) ratio $n(R)/n_{\text{rms}}$ of the edge density to the rms density; (c) center-to-edge dust optical depth $\tau(R)$; (d) ratio of peak emission measure/central emission measure. Results are for $\langle h\nu \rangle_i = 18 \text{ eV}$.

significance, but eq. (21) can be used to estimate the total H ionization rate $f_{\text{ion}}Q_0$ in dusty H II regions.

Even for large values of τ_{d0} , Fig. 6 shows that $\sim 1/3$ of the $h\nu > 13.6 \text{ eV}$ photons are absorbed by hydrogen. This contrasts with the uniform-density models of Petrosian et al. (1972), where the fraction of the $h\nu > 13.6 \text{ eV}$ photons that are absorbed by the gas goes to zero as τ_{d0} becomes large.

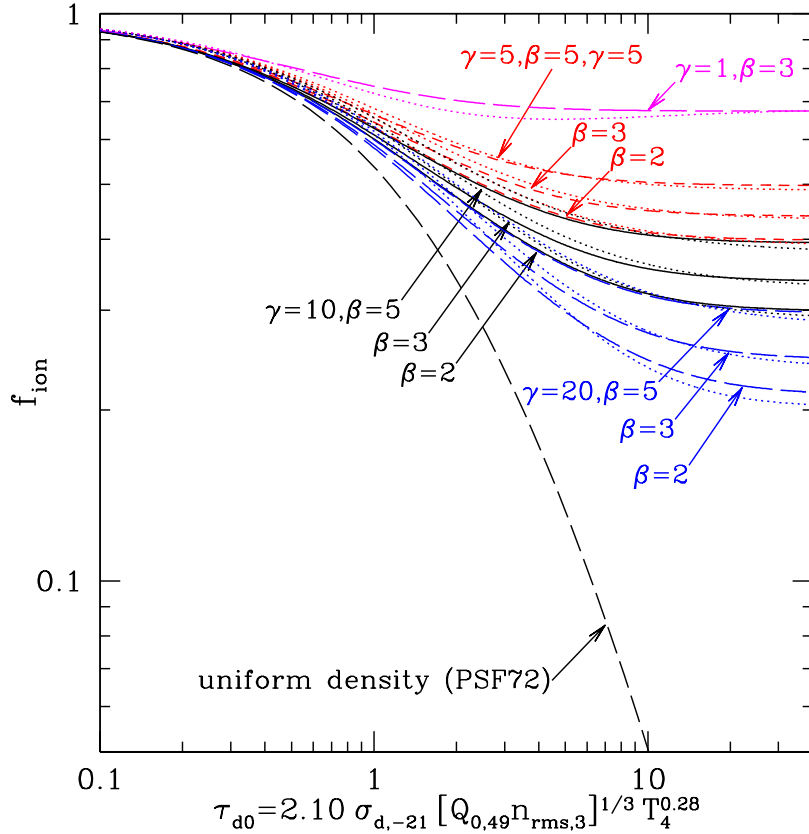


Fig. 6.— Fraction f_{ion} of the $h\nu > 13.6$ eV photons that photoionize H in dusty H II regions with radiation pressure, as a function of τ_{d0} , for $\beta = 2, 3, 5$ and $\gamma = 5, 10, 20$. Calculated assuming $\langle h\nu \rangle_i = 18$ eV. The dotted lines show the fitting formula (21) for each case. Also shown is f_{ion} calculated for assumed uniform density (Petrosian et al. 1972).

4. Dust Drift

4.1. Gas Drag vs. Radiation Pressure

Eq. (1) assumes the dust to be tightly coupled to the gas, so that the radiation pressure force on the dust can be considered to act directly on the gas. In reality, radiation pressure will drive the dust grains through the plasma. If the grains approach their terminal velocities (i.e., acceleration can be neglected) then, as before, it can be assumed that the radiation pressure force is effectively applied to the gas. However, the motion of the dust grains will lead to changes in the dust/gas ratio, due to movement of the grains from one zone to another, as well as because of grain destruction. Here we estimate the drift velocities of grains.

Let $Q_{\text{pr}}\pi a^2$ be the radiation pressure cross section for a grain of radius a . Figure 7 shows $Q_{\text{pr}}(a, \lambda)$ averaged over blackbody radiation fields with $T = 25000$ K, 32000 K, and 40000 K, for carbonaceous grains and amorphous silicate grains. For spectra characteristic of O stars, $\langle Q_{\text{pr}} \rangle \approx$

1.5 for $0.02\mu\text{m} \lesssim a \lesssim 0.25\mu\text{m}$.

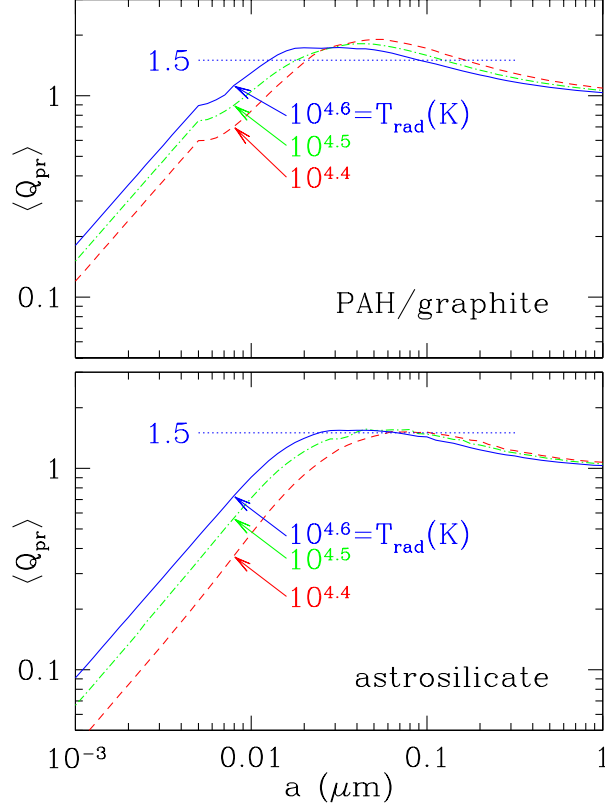


Fig. 7.— Spectrum-averaged radiation pressure efficiency factor $\langle Q_{\text{pr}} \rangle$ as a function of radius, for $T = 25000$ K, 32000 K, and 40000 K blackbody spectra. For temperatures characteristic of O stars, $\langle Q_{\text{pr}} \rangle \approx 1.5$ to within 20% for $0.02\mu\text{m} \lesssim a \lesssim 0.25\mu\text{m}$.

If the magnetic field $B = 0$, the terminal velocity v_d for a grain at distance r is determined by balancing the forces due to radiation pressure and gas drag:

$$\frac{L(r)}{4\pi r^2 c} \pi a^2 \langle Q_{\text{pr}} \rangle = 2\pi a^2 n k T G(s) \quad , \quad s \equiv \frac{v_d}{\sqrt{2kT/m_{\text{H}}}} \quad , \quad (24)$$

where the drag function $G(s)$, including both collisional drag and Coulomb drag, can be approximated by (Draine & Salpeter 1979)

$$G(s) \approx \frac{8s}{3\sqrt{\pi}} \left(1 + \frac{9\pi s^2}{64} \right)^{1/2} + \left(\frac{eU}{kT} \right)^2 \ln \Lambda \frac{s}{(3\sqrt{\pi}/4 + s^3)} \quad , \quad (25)$$

$$\Lambda = \frac{3}{2ae} \frac{kT}{|eU|} \left(\frac{kT}{\pi n_e} \right)^{1/2} = 6.6 \times 10^6 a_{-5}^{-1} \frac{kT}{|eU|} T_4^{1/2} n_3^{-1/2} \quad , \quad (26)$$

where U is the grain potential, $a_{-5} \equiv a/10^{-5}$ cm, and $n_3 \equiv n_e/10^3$ cm $^{-3}$. The drag force from the electrons is smaller than that from the ions by at least $\sqrt{m_e/m_p}$, and can be neglected. The charge

on the grains will be determined by collisional charging and photoelectric emission. Collisional charging would result in $eU/kT \approx -2.51$ (Spitzer 1968), or $U \approx -2.16T_4\text{V}$. Photoelectric charging will dominate close to the star, but is expected to result in potentials $U \lesssim 10\text{V}$. Taking $|eU/kT| \approx 2.5$ and $\ln \Lambda \approx 14.8$ as representative,

$$G(s) \approx \left[1.50 \left(1 + \frac{9\pi}{64}s^2 \right)^{1/2} + \frac{69.5}{1 + 4s^3/3\sqrt{\pi}} \right] s \quad . \quad (27)$$

Note that $G(s)$ is not monotonic: as s increases from 0, $G(s)$ reaches a peak value ~ 42 for $s \approx 0.89$, but then begins to decline with increasing s as the Coulomb drag contribution falls. At sufficiently large s , the direct collisional term becomes large enough that $G(s)$ rises above ~ 42 and continues to rise thereafter.

The drag time for a grain of density $\rho = 3 \text{ g cm}^{-3}$ in H II gas is

$$\tau_{\text{drag}} = \frac{Mv}{F_{\text{drag}}} = 295 \left(\frac{a_{-5}}{n_3 T_4^{1/2}} \right) \frac{s}{G(s)} \text{ yr} \quad . \quad (28)$$

For $n_3 \gtrsim 0.01$ this is sufficiently short that each grain can be assumed to be moving at its terminal velocity v_d , with isothermal Mach number $s \equiv v_d/\sqrt{2kT/m_{\text{H}}}$ determined by the dimensionless equation

$$G(s) = \left[\phi(y) + \beta e^{-\tau(y)} \right] \frac{u(y)}{y^2} \langle Q_{\text{pr}} \rangle \quad , \quad y \equiv \frac{r}{\lambda_0} \quad . \quad (29)$$

Eq. (29) is solved to find $s(r)$. For $20 < G < 42$, there are three values of s for which the drag force balances the radiation pressure force. The intermediate solution is unstable; we choose the smaller solution,³ which means that s undergoes a discontinuous jump from ~ 0.9 to 6.2 at $G \approx 42$. The resulting terminal velocity $v(r)$ is shown in Figure 8 for 7 values of $Q_{0,49}n_{\text{rms}}$. The velocities in the interior can be very large, but the velocities where most of the dust is located [$\tau(r)/\tau(R) > 0.5$] are much smaller.

In the outer part of the bubble, where most of the gas and dust are located, the drift velocities are much more modest. This is visible in Fig. 8a, where the drift speeds become small as $r \rightarrow R$, but is more clearly seen in Fig. 8b, showing drift speeds as a function of normalized optical depth. The range $0.5 < \tau(r)/\tau(R) < 1$ contains more than 50% of the dust, and throughout this zone the drift speeds are $\lesssim 0.3 \text{ km s}^{-1}$ even for $Q_{0,49}n_{\text{rms}}$ as large as 10^7 cm^{-3} . With drift speeds $v_d \lesssim 0.3 \text{ km s}^{-1}$, grains will not be destroyed, except perhaps by shattering in occasional collisions between grains with different drift speeds. However, for large values of n_{rms} , these grains are located close to the boundary, the drift times may be short, and the grains may be driven out of the H II and into the surrounding shell of dense neutral gas. This will be discussed further below.

³ This solution is physically relevant if the drift speed began with $s \lesssim 0.9$ and increased with time.

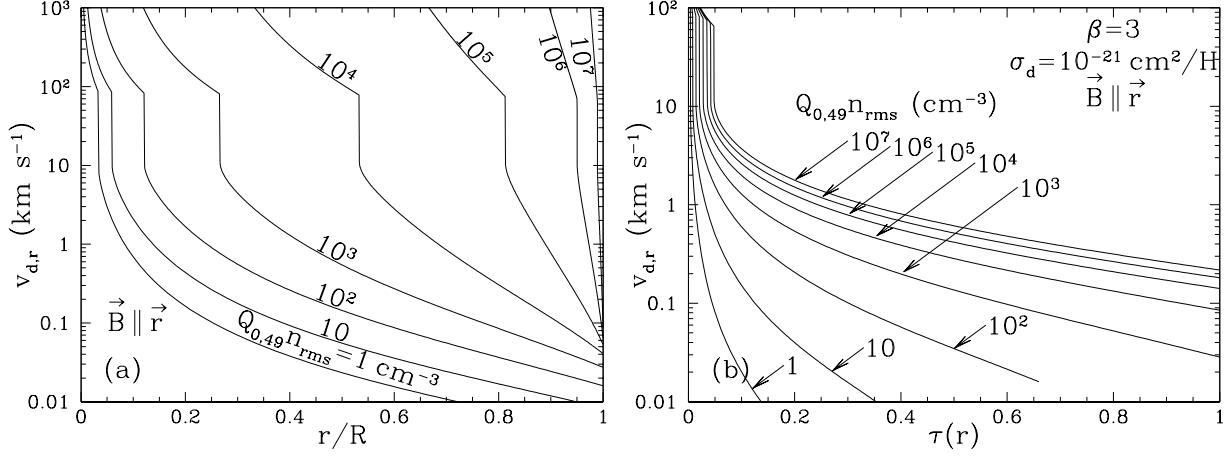


Fig. 8.— Radial drift velocities $v_{d,r}$ for six different H II regions, all with $\beta = 3$ and $\gamma = 10$, for $T_4 = 0.94$, $\langle h\nu \rangle_i = 18 \text{ eV}$, $Q_{\text{pr}} = 1.5$, $|eU/kT| = 2.5$, and $B = 0$. (a) $v_{d,r}$ vs r/R . All solutions have large drift velocities near the center, which will result in removal of the dust from the interior. Drift velocities increase with increasing $Q_0 n_{\text{rms}}$. (b) $v_{d,r}$ as a function of dust column density $\tau(r)$. Even if $B = 0$ or $\mathbf{B} \parallel \mathbf{r}$, drift velocities $v_d > 75 \text{ km s}^{-1}$ occur only in a region with a small fraction of the dust. In most of the volume, drift will not result in grain destruction.

4.2. Magnetic Fields

Let $\epsilon_B \equiv B^2/16\pi nkT$ be the ratio of magnetic pressure to gas pressure. The importance of magnetic fields for the grain dynamics is determined by the dimensionless ratio $\omega\tau_{\text{drag}}$, where $\omega \equiv QB/Mc$ is the gyrofrequency for a grain with charge Q and mass M in a magnetic field B :

$$(\omega\tau_{\text{drag}})^2 = 17.3 \frac{T_4^2}{n_3 a_{-5}^2} \left(\frac{\epsilon_B}{0.1}\right) \left(\frac{eU/kT}{2.5}\right)^2 \left(\frac{71}{G(s)/s}\right)^2, \quad \epsilon_B \equiv \left(\frac{B^2/8\pi}{2nkT}\right). \quad (30)$$

If $|eU/kT| \approx 2.5$ and $\ln \Lambda \approx 15$, then $(G(s)/s) \approx 71$ for $s \lesssim 0.5$.

Let the local magnetic field be $\mathbf{B} = B(\hat{\mathbf{r}} \cos \theta + \hat{\mathbf{y}} \sin \theta)$. The steady-state drift velocity is

$$v_d = \left(\frac{F_{\text{rad}}\tau_{\text{drag}}}{M}\right) \sqrt{\frac{1 + (\omega\tau_{\text{drag}})^2 \cos^2 \theta}{1 + (\omega\tau_{\text{drag}})^2}}, \quad (31)$$

$$v_{d,r} = \left(\frac{F_{\text{rad}}\tau_{\text{drag}}}{M}\right) \frac{1 + (\omega\tau_{\text{drag}})^2 \cos^2 \theta}{1 + (\omega\tau_{\text{drag}})^2}, \quad (32)$$

$$v_{d,y} = \left(\frac{F_{\text{rad}}\tau_{\text{drag}}}{M}\right) \frac{(\omega\tau_{\text{drag}})^2 \sin \theta \cos \theta}{1 + (\omega\tau_{\text{drag}})^2}, \quad (33)$$

$$v_{d,z} = -\left(\frac{F_{\text{rad}}\tau_{\text{drag}}}{M}\right) \frac{\omega\tau_{\text{drag}} \sin \theta}{1 + (\omega\tau_{\text{drag}})^2}, \quad (34)$$

where $v_{d,r}$, $v_{d,y}$, $v_{d,z}$ are the radial and transverse components. If $\sin \theta \rightarrow 0$, the magnetic field does not affect the radiation-pressure-driven drift velocity, but in the limit $\sin \theta \rightarrow 1$ magnetic effects can strongly suppress the radial drift if $\omega\tau_{\text{drag}} \gg 1$ and $\cos \theta \ll 1$.

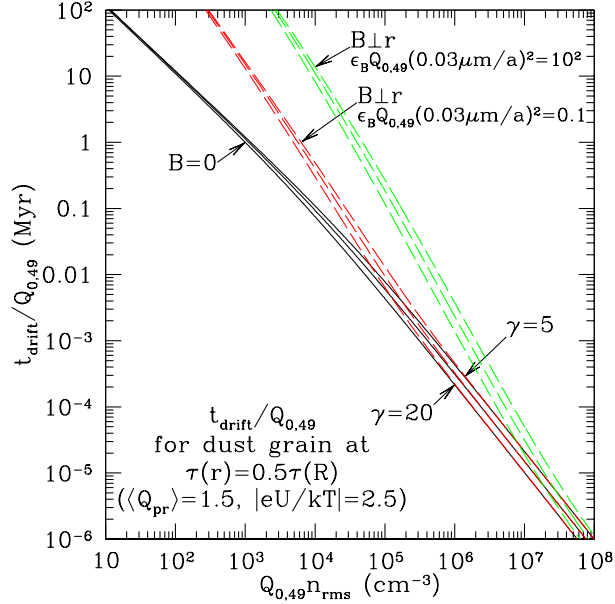


Fig. 9.— Drift timescale $t_{\text{drift}}/Q_{0,49}$ (see eq. 35) for $\beta = 3$ and $\gamma = 5, 10,$ and 20 (assuming $T_4 = 0.94$, $\langle h\nu \rangle_i = 18 \text{ eV}$). The dust grains are assumed to have $\langle Q_{\text{pr}} \rangle = 1.5$ and $|eU/kT| = 2.5$. Solid lines are for $B = 0$ (or $\mathbf{B} \parallel \mathbf{r}$). Broken lines are for $a = 0.03 \mu\text{m}$, and $\epsilon_B Q_{0,49} = 0.1$ and 10^2 .

The magnetic field strength is uncertain, but it is unlikely that the magnetic energy density will be comparable to the gas pressure; hence $\epsilon_B \lesssim 0.1$. From eq. (30) it is then apparent that if the magnetic field is strong ($\epsilon_B \approx 0.1$), magnetic effects on the grain dynamics can be important in low density H II regions, but will not be important for very high densities: $(\omega\tau_{\text{drag}})^2 \lesssim 1$ for $n_3 \gtrsim 170a_{-5}^{-2}\epsilon_B$.

4.3. Drift Timescale

When radiation pressure effects are important, the gas and dust are concentrated in a shell that becomes increasingly thin as $Q_0 n_{\text{rms}}$ is increased. The drift velocities where most of the dust is located are not large (see Fig. 8b), but the grains are also not far from the ionization front. The timescale on which dust drift would be important can be estimated by calculating the drift velocity at the radius $r_{0.5}$ defined by $\tau(r_{0.5}) = 0.5\tau(R)$. More than 50% of the dust has $r_{0.5} < r < R$. Figure 9 shows the characteristic drift time

$$t_{\text{drift}} \equiv \frac{R - r_{0.5}}{v_{d,r}(r_{0.5})} . \quad (35)$$

If no magnetic field is present, the drift velocity depends only on T and the dimensionless quantities $\{\phi, \tau, u, y, \langle Q_{\text{pr}} \rangle\}$ (see eq. 29). It is easy to see that for fixed T and $Q_0 n_{\text{rms}}$, the radius $R \propto Q_0$, thus $t_{\text{drift}} \propto Q_0$. Figure 9 shows $t_{\text{drift}}/Q_{0,49}$. For $Q_{0,49} = 1$, H II regions with $n_{\text{rms}} > 10^3 \text{ cm}^{-3}$

have $t_{\text{drift}} < 10^6$ yr if magnetic effects are negligible. If a magnetic field is present with $\mathbf{B} \perp \mathbf{r}$ and $\epsilon_B = 0.1$, then the grain drift is slowed, but drift times of < 1 Myr are found for $n_{\text{rms}} > 10^4 \text{ cm}^{-3}$. Therefore, compact and ultracompact H II regions around single O stars are able to lower the dust/gas ratio by means of radial drift of the dust on time scales of \lesssim Myr. However, if the O star is moving relative to the gas cloud with a velocity of more than a few km s^{-1} , then individual fluid elements pass through the ionized zone on timescales that may be shorter than the drift timescale, precluding substantial changes in the dust-to-gas ratio.

Grain removal by drift can also occur for giant H II regions. As an example, consider a giant H II region ionized by a compact cluster of $\sim 10^3$ O stars emitting ionizing photons at a rate $Q_0 = 10^{52} \text{ s}^{-1}$. For $n_{\text{rms}} = 10^3 \text{ cm}^{-3}$, we have $Q_{0,49} n_{\text{rms}} = 10^6 \text{ cm}^{-3}$, and we see that if $B = 0$, the drift timescale is only $t_{\text{drift}} \approx 2 \times 10^5$ yr. If a magnetic field is present with $\mathbf{B} \perp \mathbf{r}$ and $\epsilon_B = 0.1$, then from Figure 9 the drift timescale t_{drift} is increased, but only to $\sim 10^6$ yr. It therefore appears possible for radiation-pressure driven drift to remove dust from giant H II regions provided they are sufficiently dense.

Aside from magnetic effects, the drift speeds at a given location depend only on $\langle Q_{\text{pr}} \rangle$ and T_4 (see eq. 29). Figure 7 shows that $\langle Q_{\text{pr}} \rangle$ is constant to within a factor ~ 1.5 for $a \gtrsim 0.010 \mu\text{m}$. Hence radiation-pressure-drive drift would act to drive grains with $a \gtrsim 0.01 \mu\text{m}$ outwards. Smaller grains will drift as well, but more slowly. Because of this, the gas-to-dust ratio in the centers of H II regions should in general be lower than the gas-to-dust ratio in the gas prior to ionization. The dust-to-gas ratio will first be reduced in the center, where the drift speeds (see Fig. 8) are large. Dust drift will also alter the dust-to-gas ratio in the outer ionized material, initially raising it by moving dust outwards from the center. In an initially uniform neutral cloud, the ionization front expands rapidly at early times (see, e.g., Fig. 37.3 in Draine 2011) but in gas with $n_3 \gtrsim 1$, at late times the ionization front will slow to velocities small enough for dust grains to actually drift outward across the ionization front, lowering the overall dust-to-gas ratio within the H II region.

4.4. Grain Destruction

Arthur et al. (2004) computed models of uniform density H II regions including the effects of dust destruction by sublimation or evaporation, finding that the dust/gas ratio can be substantially reduced near the star. If the maximum temperature at which a grain can survive is T_{sub} , and the Planck-averaged absorption efficiencies are Q_{uv} and Q_{ir} for $T = T_\star$ and $T = T_{\text{max}}$, then grains will be destroyed within a distance r_{sub} with

$$\frac{r_{\text{sub}}}{R_{s0}} = 2.82 \times 10^{-3} L_{39}^{1/6} n_{\text{rms},3}^{2/3} \left(\frac{10^3 \text{ K}}{T_{\text{sub}}} \right)^2 \left(\frac{L_{39}}{Q_{0,49}} \right)^{1/3} \left(\frac{Q_{\text{uv}}/Q_{\text{ir}}}{10^2} \right)^{1/2} \quad (36)$$

For parameters of interest (e.g., $L_{39}/Q_{0,49} \approx 1$, $L_{39} \lesssim 10^2$) we find $r_{\text{sub}}/R_{s0} \ll 1$ for $n_{\text{rms}} \lesssim 10^5 \text{ cm}^{-3}$, and sublimation would therefore destroy only a small fraction of the dust.

As we have seen, we expect radiation pressure to drive grains through the gas, with velocity given by eq. (31). Drift velocities $v_d \gtrsim 75 \text{ km s}^{-1}$ will lead to sputtering by impacting He ions, with sputtering yield $Y(\text{He}) \approx 0.2$ for $80 \lesssim v \lesssim 500 \text{ km s}^{-1}$ (Draine 1995). For hypersonic motion, the grain of initial radius a will be destroyed after traversing a column density

$$n_{\text{H}} \Delta r = \frac{n_{\text{H}}}{n_{\text{He}}} \frac{4\rho a}{Y(\text{He})\mu} \approx 2 \times 10^{20} a_{-5} \left(\frac{Y(\text{He})}{0.2} \right) \text{ cm}^{-2} \quad (37)$$

for a grain density $\rho/\mu = 1 \times 10^{23} \text{ cm}^{-3}$, appropriate for either silicates (e.g., FeMgSiO_4 , $\rho/\mu \approx 3.8 \text{ g cm}^{-3}/25m_{\text{H}} = 9 \times 10^{22} \text{ cm}^{-3}$) or carbonaceous material ($2 \text{ g cm}^{-3}/12m_{\text{H}} = 1.0 \times 10^{23} \text{ cm}^{-3}$). Therefore the dust grain must traverse material with (initial) dust optical depth

$$\Delta\tau_d = \sigma_d n_{\text{H}} \Delta r = 0.2\sigma_{d,-21} a_{-5} \left(\frac{Y(\text{He})}{0.2} \right) \quad (38)$$

if it is to be substantially eroded by sputtering. However, Fig. 8b shows that even in the absence of magnetic effects, $v_d \gtrsim 75 \text{ km s}^{-1}$ occurs only in a central region with $\tau_d < 0.05$. Therefore sputtering arising from radiation-pressure-driven drift will not appreciably affect the dust content.

5. Discussion

5.1. Absorption of Ionizing Photons by Dust

For a sample of 13 Galactic H II regions, Inoue (2002) used infrared and radio continuum observations to obtain the values of f_{ion} shown in Figure 10. The estimated values of f_{ion} are much larger than would be expected for uniform H II regions with dust-to-gas ratios comparable to the values found in neutral clouds. Inoue (2002) concluded that the central regions of these H II regions must be dust-free, noting that this was likely to be due to the combined effects of stellar winds and radiation pressure on dust. As seen in Fig. 10, the values of f_{ion} found by Inoue are entirely consistent with what is expected for static H II regions with radiation pressure for $5 \lesssim \gamma \lesssim 20$ (corresponding to $0.5 \lesssim \sigma_{d,-21} \lesssim 2$), with no need to appeal to stellar winds or grain destruction.

5.2. The Density-Size Correlation for H II Regions

H II regions come in many sizes, ranging from H II regions powered by a single O star, to giant H II regions ionized by a cluster of massive stars. The physical size of the H II region is obviously determined both by the total ionizing output Q_0 provided by the ionizing stars, and the r.m.s. density n_{rms} of the ionized gas, which is regulated by the pressure p_{edge} of the confining medium. With the balance between photoionization and recombination determining the size of an H II region, an anticorrelation between size D and density n_{rms} is expected, and was observed as soon as large samples of H II regions became available (e.g., Habing & Israel 1979; Kennicutt 1984).

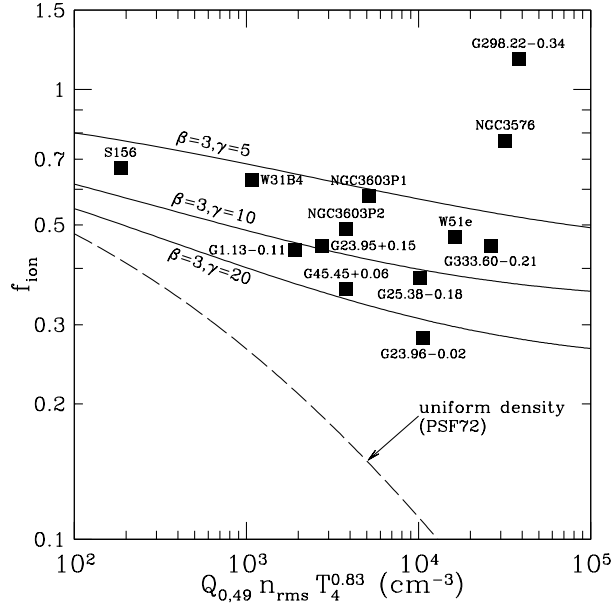


Fig. 10.— Photoionizing fraction f_{ion} for 12 Galactic H II regions, as estimated by Inoue (2002) from infrared and radio observations, vs. $Q_{0,49} n_e T_4^{0.83}$ (see text). f_{ion} cannot exceed 1, therefore the high value found for G298.22-0.34 give some indication of the uncertainties in estimation of f_{ion} . Solid lines: f_{ion} for H II regions with radiation pressure for dust characterized by $\gamma = 5, 10$, and 20 . Broken line: f_{ion} for uniform H II regions with $\sigma_d = 10^{-21} \text{ cm}^2 \text{ H}^{-1}$.

For dustless H II regions, one expects $n_{\text{rms}} \propto D^{-1.5}$ for fixed Q_0 , but for various samples relations close to $n_{\text{rms}} \propto D^{-1}$ were reported (e.g., Garay et al. 1993; Garay & Lizano 1999; Kim & Koo 2001; Martín-Hernández et al. 2005). For ultracompact H II regions, Kim & Koo (2001) attribute the $n_e \propto D^{-1}$ trend to a “champagne flow” and the hierarchical structure of the dense gas in the star-forming region, but Arthur et al. (2004) and Dopita et al. (2006) argue that the $n_e \propto D^{-1}$ trend is a result of both absorption by dust and radiation pressure acting on dust in static H II regions.

Hunt & Hirashita (2009) recently reexamined the size-density relationship. They interpreted the size-density relation for different observational samples in terms of models with different star formation rates [and hence different time evolution of the ionizing output $Q_0(t)$], and differences in the density of the neutral cloud into which the H II region expands. Their models did not include the effects of radiation pressure on dust; at any time the ionized gas in an H II region was taken to have uniform density, resulting in overestimation of the dust absorption.

Figure 11a shows a grid of n_{rms} vs. D for the present models, for four combinations of (β, γ) . While differences between the models with different (β, γ) can be seen, especially for high Q_0 and high p_{edge} , the overall trends are only weakly dependent on β and γ , at least for $1 \lesssim \gamma \lesssim 20$.

Figure 11b shows the model grid for $\beta = 3$ and $\gamma = 5$ together with observed values of D and n_{rms} from a number of different studies. It appears that observed H II regions – ranging from H II

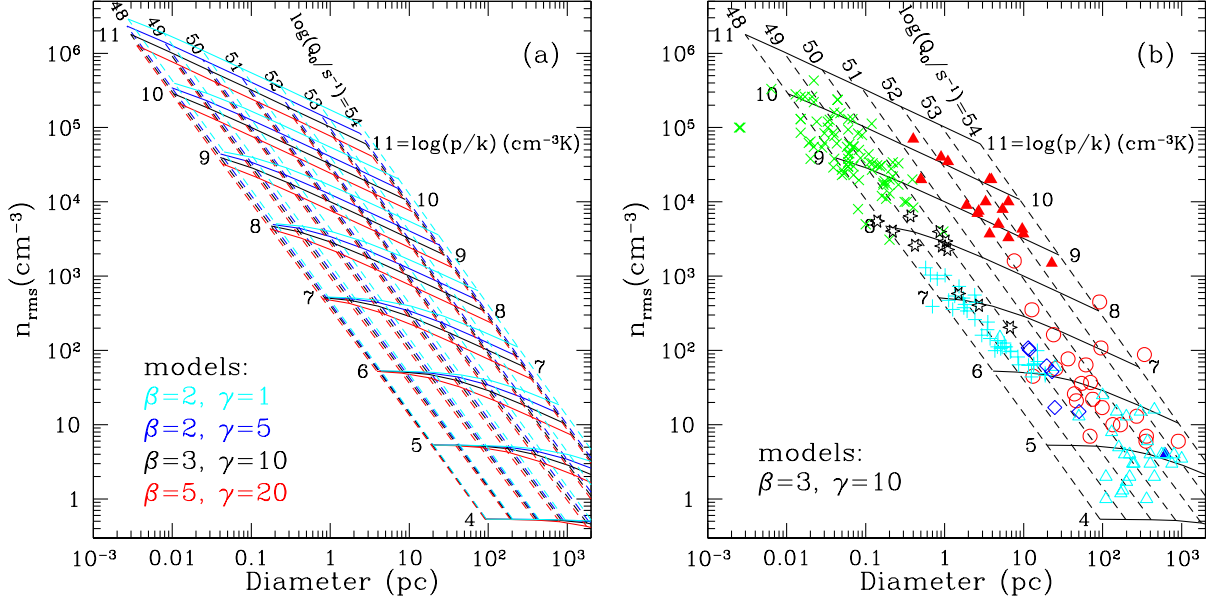


Fig. 11.— Density n_{rms} vs. diameter D . (a) Models with $(\beta, \gamma) = (2, 1)$, $(2, 5)$, $(3, 10)$, and $(5, 20)$. Results shown were calculated for $T_4 = 0.94$, $\langle h\nu \rangle_i = 18 \text{ eV}$. Solid lines show models with p_{edge} fixed, and Q_0 varying from 10^{48} s^{-1} to 10^{54} s^{-1} . Broken lines show models with Q_0 fixed, and p_{edge}/k varying from $10^4 \text{ cm}^{-3} \text{ K}$ to $10^{11} \text{ cm}^{-3} \text{ K}$. (b) Model grid for $\beta = 3$, $\gamma = 10$ together with observed values are shown for various samples of Galactic and extragalactic H II regions. Cyan open triangles: Kennicutt (1984). Blue diamonds: Churchwell & Goss (1999). Green crosses: Garay & Lizano (1999). Cyan crosses: Kim & Koo (2001). Black open stars: Martín-Hernández et al. (2005). Red solid triangles: radio sample from Hunt & Hirashita (2009). Red open circles: HST sample from Hunt & Hirashita (2009).

regions ionized by one or at most a few O stars ($Q_0 < 10^{50} \text{ s}^{-1}$) to “super star clusters” powered by up to $10^3 - 10^5$ O stars ($Q_0 = 10^{52} - 10^{54} \text{ s}^{-1}$) can be accommodated by the present static equilibrium models with external pressures in the range $10^4 \lesssim p/k \lesssim 10^{10.3} \text{ cm}^{-3} \text{ K}$. Note that for diameters $D \gtrsim 10^2 \text{ pc}$, the assumption of static equilibrium is unlikely to be justified, because the sound-crossing time $(D/2)/15 \text{ km s}^{-1} \gtrsim 3 \text{ Myr}$ becomes longer than the lifetimes of high-mass stars.

The fact that some H II region samples (e.g., Garay et al. 1993; Kim & Koo 2001) seem to obey a $n_{\text{rms}} \propto D^{-1}$ relationship appears to be an artifact of the sample selection. We see in Fig. 11b that the overall sample of H II regions does not have a single n_{rms} -vs.- D relationship. But the observations appear to be generally consistent with the current models of dusty H II regions.

5.3. Cavities in H II Regions: N49

Even without dust present, radiation pressure from photoelectric absorption by H and He can alter the density profile in a static H II region, lowering the central density and enhancing the density near the edge of the ionized region (see Fig. 2a). As seen in Figure 4a, for large values of $Q_0 n_{\text{rms}}$ the surface brightness profile can be noticeably flattened. If dust is assumed to be present, with properties typical of the dust in diffuse clouds, the equilibrium density profile changes dramatically, with a central cavity surrounded by a high-pressure shell of ionized gas pushed out by radiation pressure. In real H II regions, fast stellar winds will also act to inflate a low-density cavity, or “bubble”, near the star; the observed density profile will be the combined result of the stellar wind bubble and the effects of radiation pressure.

The GLIMPSE survey (Churchwell et al. 2009) has discovered and catalogued numerous interstellar “bubbles”. An example is N49 (Watson et al. 2008), with a ring of free-free continuum emission at 20 cm, surrounded by a ring of $8\mu\text{m}$ PAH emission. An O6.5V star is located near the center of the N49 ring. The image is nearly circularly symmetric, with only a modest asymmetry that could be due to motion of the star relative to the gas. The 20 cm image has a ring-peak-to-center intensity ratio $I(\text{peak})/I(\text{center}) \approx 2$.

Is the density profile in N49 consistent with what is expected for radiation pressure acting on dust? From the 2.89 Jy flux from N49 at $\lambda = 20$ cm (Helfand et al. 2006) and distance 5.7 ± 0.6 kpc (Churchwell et al. 2006), the stellar source has $Q_{0,49} \approx (0.78 \pm 0.16)/f_{\text{ion}}$. If $f_{\text{ion}} \approx 0.6$, then $Q_{0,49} \approx (1.3 \pm 0.3)$. The H II region, with radius (0.018 ± 0.02) deg, has $n_{\text{rms}} \approx 197 \pm 63 \text{ cm}^{-3}$. Hence $Q_{0,49} n_{\text{rms}} \approx 260 \text{ cm}^{-3}$. If $\sigma_{d,-21} = 1$, then $\tau_{d0} \approx 1.3$. From Fig. 6a we confirm that $f_{\text{ion}} \approx 0.6$ for $\tau_{d0} \approx 1.3$.

Figure 5d shows that an H II region with $\tau_{d0} = 1.3$ is expected to have a central minimum in the emission measure, but with $I(\text{peak})/I(\text{center}) \approx 1.3$ for $\beta = 3, \gamma = 10$, whereas the observed $I(\text{peak})/I(\text{center}) \approx 2$. The central cavity in N49 is therefore significantly larger than would be expected based on radiation pressure alone. While the effects of radiation pressure are not negligible in N49, the observed cavity must be the result of the combined effects of radiation pressure and a dynamically-important stellar wind (which is of course not unexpected for an O6.5V star).

5.4. Lyman- α

The original ionizing photon deposits a radial momentum $h\nu_i/c$ at the point where it is absorbed by either a neutral atom or a dust grain. A fraction $(1 - f_{\text{ion}})$ of the ionizing photons are absorbed by dust; this energy is reradiated isotropically, with no additional force exerted on the emitting material. Because the infrared optical depth within the H II region is small, the infrared emission escapes freely, with no dynamical effect within the H II region.

A fraction f_{ion} of the ionizing energy is absorbed by the gas. Subsequent radiative recomb-

nation and radiative cooling converts this energy to photons, but the isotropic emission process itself involves no net momentum transfer to the gas. We have seen above that the H II can have a center-to-edge dust optical depth $\tau(R) \approx 1.6$ for $\tau_{d0} \gtrsim 5$, or $Q_{0,49}n_{\text{rms}} \gtrsim 10^2 \text{ cm}^{-3}$ (cf. Fig. 5c with $\beta = 3$, $\gamma = 10$). This optical depth applies to the $h\nu > 13.6 \text{ eV}$ ionizing radiation; the center-to-edge optical depth for the $h\nu < 3.4 \text{ eV}$ Balmer lines and collisionally-excited cooling lines emitted by the ionized gas will be significantly smaller, and much of this radiation will escape dust absorption or scattering within the H II region. That which is absorbed or scattered will exert a force on the dust at that point only to the extent that the diffuse radiation field is anisotropic. We conclude that momentum deposition from the Balmer lines and collisionally-excited cooling lines within the ionized zone will be small compared to the momentum deposited by stellar photons.

Lyman- α is a special case. At low densities ($n \ll 10^3 \text{ cm}^{-3}$), $\sim 70\%$ of Case B recombinations result in emission of a Ly- α photon, increasing to $> 95\%$ for $n > 10^5 \text{ cm}^{-3}$ as a result of collisionally-induced $2s \rightarrow 2p$ transitions (Brown & Mathews 1970). After being emitted isotropically, the photon may scatter many times before either escaping from the H II or being absorbed by dust. Most of the scatterings take place near the point of emission, while the photon frequency is still close to line-center. On average, the net radial momentum transfer per emitted photon will likely be dominated by the last scattering event before the photon escapes from the H II region, or by the dust absorption event if it does not. At a given point in the nebula, the incident photons involved in these final events will be only moderately anisotropic. Since there is less than one Ly- α photon created per case B recombination, the total radial momentum deposited by these final events will be a small fraction of the radial momentum of the original ionizing photons. Henney & Arthur (1998) estimate that dust limits the Ly- α radiation pressure to $\sim 6\%$ of the gas pressure. We conclude that Ly- α has only a minor effect on the density profile within the ionized zone.

5.5. H II Region Expansion

H II regions arise when massive stars begin to emit ionizing radiation. The development of the H II region over time depends on the growth of the ionizing output from the central star, and the expansion of the initially-high pressure ionizing gas. Many authors (e.g., Kahn 1954; Spitzer 1978) have discussed the development of an H II region in gas that is initially neutral and uniform. If the ionizing output from the star turns on suddenly, the ionization front is initially “strong R-type”, propagating supersonically without affecting the density of the gas, slowing until it becomes “R-critical”, at which point it makes a transition to “D-type”, with the ionization front now preceded by a shock wave producing a dense (expanding) shell of neutral gas bounding the ionized region.

While the front is R-type, the gas density and pressure are essentially uniform within the ionized zone. When the front becomes D-type, a rarefaction wave propagates inward from the ionization front, but the gas pressure (if radiation pressure effects are not important) remains relatively uniform within the ionized region, because the motions in the ionized gas are subsonic.

When radiation pressure effects are included, the instantaneous density profile interior to the ionization front is expected to be similar to the profile calculated for the static equilibria studied here. Let V_i be the velocity of the ionization front relative to the star. When the ionization front is weak D-type, the velocity of the ionization front relative to the ionized gas just inside the ionization front is $\sim 0.5V_i$ (Spitzer 1978). Given the small dust drift velocities $v_{d,r}$ near the ionization front (i.e., $\tau(r) \rightarrow \tau(R)$ in Fig. 8), dust is unable to drift outward across the ionization front as long as the ionization front is propagating outward with a speed (relative to the ionized gas) $V_i \gtrsim 0.1 \text{ km s}^{-1}$.

6. Summary

1. Dusty H II regions in static equilibrium consist of a three-parameter family of similarity solutions, parametrized by parameters β , γ , and a third parameter, which can be taken to be $Q_{0,49}n_{\text{rms}}$ or τ_{d0} (see eq. 16). The β parameter (eq. 6) characterizes the relative importance of $h\nu < 13.6 \text{ eV}$ photons, and γ (eq. 7) characterizes the dust opacity. A fourth parameter – e.g., the value of n_{rms} or $Q_{0,49}$ – determines the overall size and density of the H II region.
2. Radiation pressure acting on both gas and dust can strongly affect the structure of H II regions. For dust characteristic of the diffuse ISM of the Milky Way, static H II regions with $Q_{0,49}n_{\text{rms}} \lesssim 10^2 \text{ cm}^{-3}$ will have nearly uniform density, but when $Q_{0,49}n_{\text{rms}} \gg 10^2 \text{ cm}^{-3}$, radiation pressure acts to concentrate the gas in a spherical shell.
3. For given β and γ , the importance of radiation pressure is determined mainly by the parameter τ_{d0} (see eq. 16). When $\tau_{d0} \gtrsim 1$, radiation pressure will produce a noticeable central cavity.
4. If the dust-to-gas ratio is similar to the value in the Milky Way, then compression of the ionized gas into a shell limits the characteristic ionization parameter: $U_{1/2} \lesssim 0.01$, even for $Q_0n_{\text{rms}} \gg 1$ (see Fig. 3).
5. For $\tau_{d0} \gtrsim 1$, compression of the gas and dust into an ionized shell leads to a substantial *increase* (compared to the estimate by Petrosian et al. 1972) in the fraction f_{ion} of $h\nu > 13.6 \text{ eV}$ photons that actually ionize H, relative to what would have been estimated for a uniform density H II region, as shown in Fig. 6. Eq. (21) allows f_{ion} to be estimated for given Q_0n_{rms} , β , and γ . Galactic H II regions appear to have values of f_{ion} consistent with the present results for H II regions with radiation pressure (see Fig. 10).
6. Interstellar bubbles surrounding O stars are the result of the combined effects of radiation pressure and stellar winds. For the N49 bubble, as an example, the observed ring-like free-free emission profile is more strongly peaked than would be expected from radiation pressure alone, implying that a fast stellar wind must be present to help create the low-density central cavity.
7. For static H II regions, dust drift would be important on time scales $\lesssim 1 \text{ Myr}$ for $Q_{0,49}n_{\text{rms}} \gtrsim 10^3 \text{ cm}^{-3}$. Real H II regions are not static, and the dust will not drift out of the ionized gas

because the ionization front will generally be propagating (relative to the ionized gas just inside the ionization front) faster than the dust drift speed $\lesssim 1 \text{ km s}^{-1}$ (see Fig. 8).

I am grateful to Bob Benjamin and Leslie Hunt for helpful discussions, to R.H. Lupton for making available the SM graphics package, and to the anonymous referee for suggestions that improved the paper. This research made use of NASA's Astrophysics Data System Service, and was supported in part by NASA through JPL contract 1329088, and in part by NSF grant AST 1008570.

REFERENCES

- Arthur, S. J., Kurtz, S. E., Franco, J., & Albarrán, M. Y. 2004, *ApJ*, 608, 282
- Brown, R. L., & Mathews, W. G. 1970, *ApJ*, 160, 939
- Churchwell, E., et al. 2009, *PASP*, 121, 213
- Churchwell, E., & Goss, W. M. 1999, *ApJ*, 514, 188
- Churchwell, E., et al. 2006, *ApJ*, 649, 759
- Dopita, M. A., et al. 2006, *ApJ*, 639, 788
- Dopita, M. A., Groves, B. A., Sutherland, R. S., & Kewley, L. J. 2003, *ApJ*, 583, 727
- Draine, B. T. 1995, *Ap&SS*, 233, 111
- . 2011, *Physics of the Interstellar and Intergalactic Medium* (Princeton, NJ: Princeton University Press)
- Draine, B. T., & Salpeter, E. E. 1979, *ApJ*, 231, 77
- Gail, H. P., & Sedlmayr, E. 1979, *A&A*, 77, 165
- Garay, G., & Lizano, S. 1999, *PASP*, 111, 1049
- Garay, G., Rodriguez, L. F., Moran, J. M., & Churchwell, E. 1993, *ApJ*, 418, 368
- Habing, H. J., & Israel, F. P. 1979, *ARA&A*, 17, 345
- Helfand, D. J., Becker, R. H., White, R. L., Fallon, A., & Tuttle, S. 2006, *AJ*, 131, 2525
- Henney, W. J., & Arthur, S. J. 1998, *AJ*, 116, 322
- Hunt, L. K., & Hirashita, H. 2009, *A&A*, 507, 1327
- Inoue, A. K. 2002, *ApJ*, 570, 688

- Kahn, F. D. 1954, *Bull. Astron. Inst. Netherlands*, 12, 187
- Kennicutt, Jr., R. C. 1984, *ApJ*, 287, 116
- Kim, K., & Koo, B. 2001, *ApJ*, 549, 979
- Krumholz, M. R., & Matzner, C. D. 2009, *ApJ*, 703, 1352
- Martín-Hernández, N. L., Vermeij, R., & van der Hulst, J. M. 2005, *A&A*, 433, 205
- Martins, F., Schaerer, D., & Hillier, D. J. 2005, *A&A*, 436, 1049
- Mathews, W. G. 1967, *ApJ*, 147, 965
- . 1969, *ApJ*, 157, 583
- Petrosian, V., Silk, J., & Field, G. B. 1972, *ApJ*, 177, L69
- Savedoff, M. P., & Greene, J. 1955, *ApJ*, 122, 477
- Spitzer, L. 1968, *Diffuse matter in space* (New York: Interscience)
- . 1978, *Physical Processes in the Interstellar Medium* (New York: Wiley)
- Strömgren, B. 1939, *ApJ*, 89, 526
- Watson, C., et al. 2008, *ApJ*, 681, 1341
- Weingartner, J. C., & Draine, B. T. 2001, *ApJ*, 548, 296
- Zubko, V., Dwek, E., & Arendt, R. G. 2004, *ApJS*, 152, 211